IET Power Electronics

Special Issue on Converters and Semiconductor Circuit Breakers for HVDC and DC Grids

IET Journals
The Institution of Engineering and Technology

Successful fault current interruption on DC circuit breaker

ISSN 1755-4535
Received on 18th May 2015
Revised on 20th August 2015
Accepted on 13th September 2015
doi: 10.1049/iet-pel.2015.0351
www.ietdl.org

Yunhai Shan[1], Tee C. Lim[2] ✉, Barry W. Williams[2], Stephen J. Finney[2]

[1]*State Grid Smart Grid Research Institute, Floor 9, Building B, Future Technology Park, Changping District, Beijing 102200, People's Republic of China*
[2]*Department of Electronic & Electrical Engineering, Institute for Energy & Environment, University of Strathclyde, Royal College Building, 204 George Street, Glasgow G1 1XW, UK*
✉ *E-mail: ceetcl@eee.strath.ac.uk*

Abstract: This study focus on the interruption capability of the DC circuit breaker employing a current commutation approach and evaluates the two main factors that determine the success rate for breaker current interruption, namely the current slope d*i*/d*t* before current zero and the rate of rise of the transient recovery voltage d*v*/d*t* across the mechanical breaker contacts after current zero. A vacuum circuit breaker is used to evaluate DC breaker characteristics. Detailed mathematical and graphical analysis are presented for the proposed circuit operation used in analysing the circuit breaker properties, with simulation and experimental results at fault current levels up to 330 A.

1 Introduction

Current interruption in a direct current (DC) system is more difficult than in an alternating current (AC) system due to the absence of a natural current zero (CZ). Since there is no large inductive device in the voltage source converter-based DC system, DC breakers have to interrupt the fault current quickly to avoid excessive overcurrent and to dissipate the stored magnetic energy without producing an excessive high voltage. Numerous proposals for introducing CZ have been presented in articles and patent applications [1–9]. The methodology can be divided into two groups. The first group can be addressed as the inverse voltage method where the classic mechanical AC interrupter creates arc voltage significantly in excess of the system voltage. The second group can be interpreted as employing a current commutation method where a virtual CZ is developed by utilising auxiliary means which include current oscillation and voltage commutation; where the current oscillation is accomplished by switching parallel commutation circuits to produce a counter-current through the breaker. Voltage commutation means the current commutation is achieved by introducing a voltage which exceeds the on-state voltage of the parallel commutation path.

Asea Brown Boveri Ltd (ABB) has proposed a hybrid DC breaker to fulfil high-voltage DC (HVDC) grid requirements [10, 11]. This new hybrid configuration has negligible on-state power losses and provides current interruption capability within 4 ms, at 70 kV. There are two parallel branches: one branch contains a series combination of a semiconductor-based commutation switch and a fast mechanical disconnector, and the other branch is the semiconductor-based breaker that comprises several sections each with individual arrester banks. Each independent section in the breaker branch is designed for pro rata full voltage and full current breaking capability, whereas the load commutation switch branch is dimensioned for lower voltage and energy capability. The disconnecting circuit offers dielectric separation of the load after fault clearance thereby protecting the arrester banks of the hybrid HVDC breaker from thermal overload. The fast mechanical switch is opened with zero current thereby facilitating a lightweight contact system. When the mechanical switch reaches the open position the main HVDC breaker interrupts the current that has been commutated into it. The dielectric separation means the load commutation switch has a low voltage requirement. Proactive control of the hybrid HVDC breaker is utilised to compensate for the time delay of the fast disconnector. Another method [12–15] to produce CZ in the mechanical switch involves current oscillation. In general, this topology comprises two mechanical switches; a main breaker and an isolation switch (as with the ABB hybrid breaker); the main breaker is parallelly connected to commutation and energy absorbing paths. The main breaker supports the continuous current flow; the isolation switch provides dielectric separation of the load after fault clearance thereby avoiding metal oxide varistor (MOV) thermal overload, while the solid-state switches in the commutation path only conduct during the interruption process. A series combination of a capacitance C and inductance L is incorporated into the commutation path; thus there will be an oscillating current between the main breaker and commutation path. The line current originally flowing through the main breaker is sinusoidally transferred into the commutation path. At this point, a CZ arises in the nominal path and the main breaker can interrupt with zero current. As the line current continues to flow through the LC commutation circuit, the voltage across the capacitor C charges to a voltage within the capability of the grid. At this voltage, the remaining energy stored in the line inductance is dissipated in the energy absorption path (MOV), forcing the line current to decrease. There are two current commutation modes; namely active commutation if C is pre-charged, otherwise passive commutation.

The current oscillation approach, especially active commutation, dominates the development of the hybrid HVDC breaker. Since the current oscillation involves an arc situation, the vacuum interrupter becomes the prefer building block for HVDC circuit breakers (CBs) due to its excellent insulating properties after the CZ. However, this is not the approach proposed by ABB in [10]. Rather than interruption with an arc based on current oscillation, the ABB approach is interruption without an arc voltage. Assuming interruption at same power rating, the two approaches (traditional and ABB approaches) compare as follows:

- The mass of mechanical switch in the traditional approach is large compared with the ABB approach. Therefore, the ABB opening speed can be faster.
- Since the first approach has to deal with an arc, the interruption performance is uncertain, unlike the ABB approach.

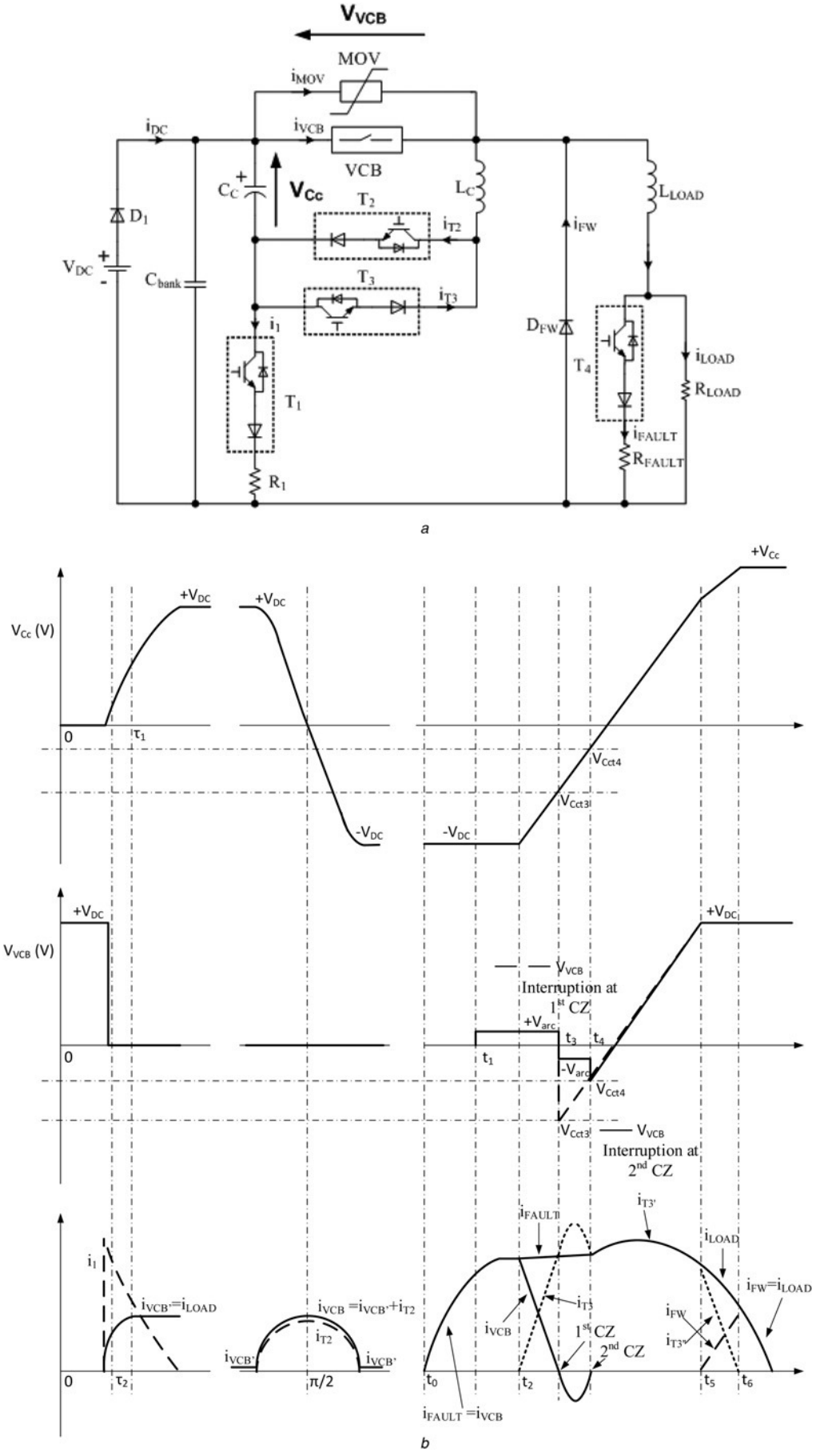

Fig. 1 *Proposed unipolar test circuit and its operational sequences*

a Proposed unipolar test circuit
b Operational sequence of the test circuit; CZ crossing in the VCB

IET Power Electron., 2016, Vol. 9, Iss. 2, pp. 207–218

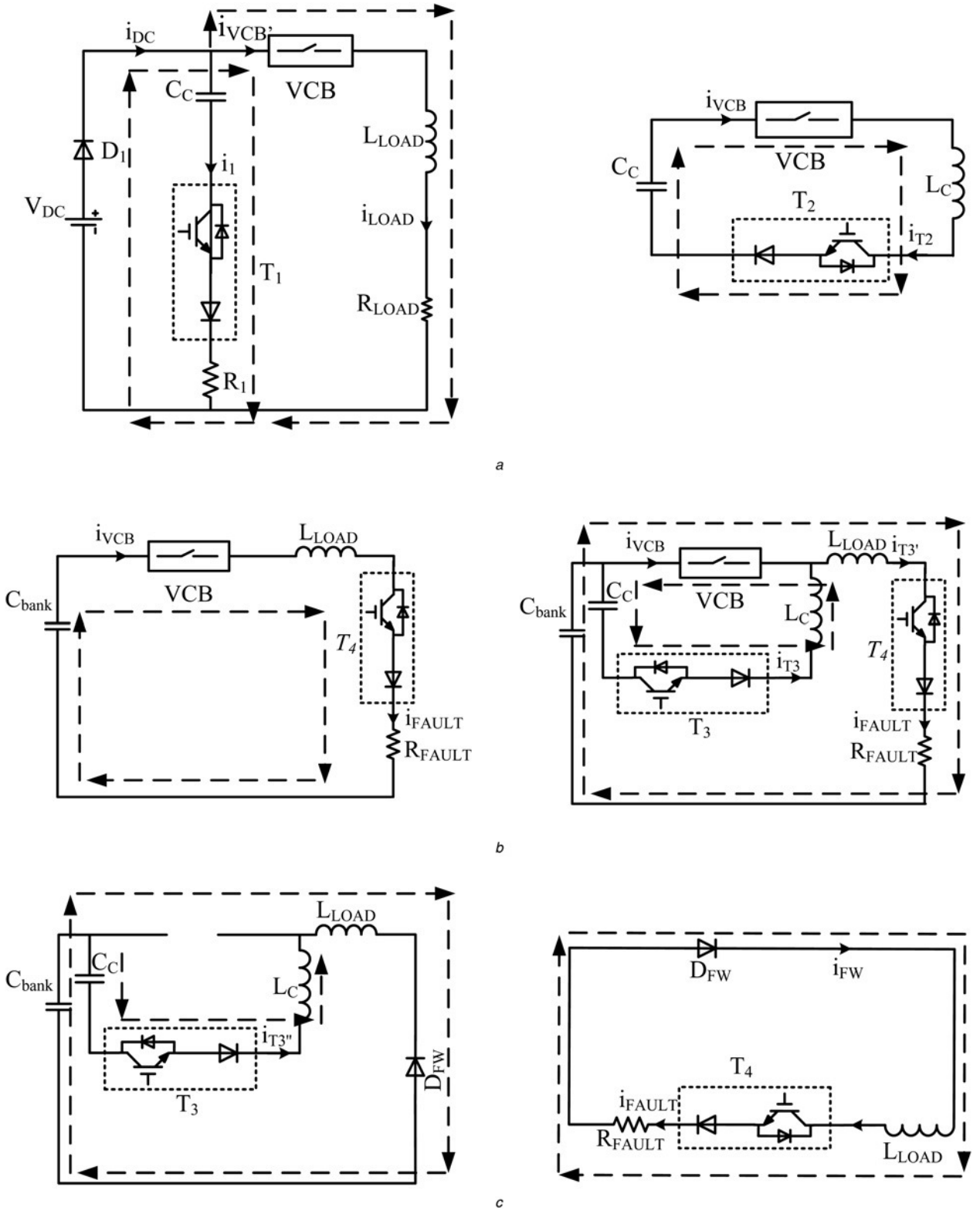

Fig. 2 *Test interruption sequences*

a Pre-charging of the commutation capacitor
b Activation of the fault by switching T_4
c Commutation of the VCB by switching T_3

- The conduction power loss in the traditional approach is smaller, but both are negligible.
- Both need solid-state switches in the commutation bypass path, and the traditional approach needs large capacitance.

For interruption at high power rating, the hybrid HVDC breaker proposed by ABB appears the only way to meet the requirement of HVDC grids. However, from an economical view, the hybrid HVDC breaker adopting current commutation may be more suitable for the low- and medium-voltage applications, such as electric traction, various drives and converter systems. This paper focus on the interruption capability of the DC CB under a current commutation approach and evaluates the two main factors that determine the success rate for breaker interruption, namely the

Table 1 Switched timing regulations

Stage	Time	VCB	T_1	T_2	T_3	T_4
resetting the commutation circuit	t_{nor}	on	on	Off	off	off
	t_{0-}	on	off	on	off	off
fault current introduction	t_0	on	off	off	off	on
VCB current interruption	t_1	off	off	off	off	on
	t_2–t_6	off	off	off	on	on

t_{nor} represents a normal working period; t_{0-} is the moment immediately following the occurrence of the peak in the coil current; t_0 represents the moment that the fault current starts to arise in the circuit; t_1 represents the moment that the VCB electrodes start to separation; and t_2–t_6 is the commutation and interruption of the fault current.

current slope di/dt before CZ and the rate of rise of the transient recovery voltage dv/dt across the mechanical breaker after CZ. As such, this paper is applicable to any LC resonant approach, including the self-sustaining, multi resonant cycle approach in [12–15].

Section 2 in this paper evaluates the proposed test circuit used to investigate the vacuum CB (VCB) characteristics. Sections 3 and 4 include the simulation and experimental results that evaluate the factors that contribute to unsuccessful and successful breaker interruption.

2 Proposed test circuit

An accurate VCB model is complicated, since it involves many parameters including contact material, gap distance and electrodes dimension. A small change in any parameter can result in a significant performance change. There is no complete mathematic model describing all VCB properties in terms of its internal parameters. Here, the VCB will be considered as a black box, ignoring all the internal parameters, but this black box will attempt to retain the features and regular pattern of successful VCB interruptions based on external conditions. There are two specific external parameters that determine this functionality; namely di/dt and dv_{VCB}/dt, where the former represents the rate of decrease of current through the VCB immediately before a CZ and the later represents the rate of increase of voltage across the VCB contacts immediately after a CZ. For example, in obtaining a 100% successful interruption rate with fast commutation, an increase in di/dt introduces a decreased allowable dv_{VCB}/dt. For fixed di/dt, dv_{VCB}/dt and arcing time, the interruption probability reduces as the interruption current increases. The di/dt and dv_{VCB}/dt for successful interruption reduce with decreasing electrode spacing [16–18]. Thus, in order to investigate VCB characteristics, a unipolar test circuit is proposed based on a VCB with active mode commutation. (Note the test circuit is not necessarily the topology that would be used for a practical hybrid DC CB — rather this proposed circuit is used in this paper to evaluate the VCB characteristics only). Fig. 1 shows the proposed unipolar test circuit and the timing intervals for commencing a fault current and subsequent breaker interruption (respective test interruption sequences are shown in Fig. 2).

There are three operating sequences during the cycle.

- Pre-charging of the commutation capacitor (resetting the commutation circuit).
- Creation of the fault by load switching T_4 (fault current introduction).
- Commutation of the VCB by switching T_3 (VCB current interruption).

The sequential timing operations for the test circuit shown in Fig. 2 are tabulated in Table 1.

2.1 Pre-charging of the commutation capacitor

Fig. 2*a* illustrates the normal operation of the test circuit (t_{nor}). To investigate VCB properties in high-current situations, the capacitor bank (C_{bank}) is charged to V_{DC} in order to supply a fault current determined by the fault resistor R_{FAULT}, which is connected in parallel with the load resistor R_{LOAD} by switch T_4. When the VCB is in an on-state (zero contact gap), a low current V_{DC}/R_{LOAD} is supplied by V_{DC}. The switches T_2, T_3 and T_4 are off and T_1 is on, charging the commutation capacitor to V_{DC} with an exponential growth via the resistor R_1. In this interval, the equation relating currents i_{DC}, $i_{VCB'}$ and i_1 is

$$i_{DC} = i_{VCB'} + i_1 \tag{1}$$

where the circuit loop of i_1 is V_{DC}–D_1–C_C–T_1–R_1 which has the following differential equation

$$\frac{1}{C_C}\int^{i_1} \mathrm{d}t + i_1 R_1 = V_{DC} \tag{2}$$

with the initial condition

$$V_{C_C} = 0 \quad \text{(V)}$$

which yields

$$i_1(t) = \frac{V_{DC}}{R_1} e^{(-t/\tau_1)} \quad \text{(A)} \tag{3}$$

and

$$V_{C_C}(t) = V_{DC}\left(1 - e^{(-t/\tau_1)}\right) \quad \text{(V)} \tag{4}$$

where $\tau_1 = R_1 C_C$

When the current i_1 reduces to zero, the voltage across the commutation capacitor C_C reaches V_{DC}, retaining this voltage provided T_1 remains on.

The circuit loop $i_{VCB'}$ comprising V_{DC}–D_1–VCB–L_{LOAD}–R_{LOAD} gives

$$L_{LOAD}\frac{\mathrm{d}i_{VCB'}}{\mathrm{d}t} + i_{VCB'}R_{LOAD} = V_{DC} \tag{5}$$

with the initial condition

$$i_{VCB'} = 0 \quad \text{(A)}$$

which yields

$$i_{VCB'}(t) = i_{LOAD}(t) = \frac{V_{DC}}{R_{LOAD}}\left(1 - e^{(-t/\tau_2)}\right) \quad \text{(A)} \tag{6}$$

where $\tau_2 = L_{LOAD}/R_{LOAD}$

When (6) stabilises, the current $i_{VCB'}$ through the VCB is equal to the source current i_{DC}. With large load resistance, this 'wetting' current is small during this interval and can be neglected in the following analysis.

Although the voltage V_{C_C} across the commutation capacitor C_C has been charged to the DC source, it is not ready to introduce a counter-current through the VCB due to its voltage polarity, V_{C_C}. The pre-charge cycle needs to be completed before the fault current is applied. The voltage polarity of the commutation capacitor has to be reversed before t_0 at t_{0-}. With T_1 off and T_2 on, the circuit loop equation for C_C–VCB–L_C–T_2 is

$$\frac{1}{C_C}\int^{i_{T_2}} \mathrm{d}t + L_C\frac{\mathrm{d}i_{T_2}}{\mathrm{d}t} = 0 \tag{7}$$

with the initial conditions

$$i_{T_2} = 0 \ \text{(A)} \quad \text{and} \quad V_{C_C} = -V_{DC} \ \text{(V)}$$

IET Power Electron., 2016, Vol. 9, Iss. 2, pp. 207–218

which yield

$$i_{T_2}(t) = \frac{V_{DC}}{Z}\sin\omega_0 t \quad \text{(A)} \tag{8}$$

and

$$\begin{gathered} V_{C_C}(t) = -V_{DC}\cos\omega_0 t \quad \text{(V)} \\ 0 \le \omega_0 t \le \pi \quad (rad) \end{gathered} \tag{9}$$

where $\omega_0 = 1/\sqrt{L_C C_C}$ (rad/s) and $Z = \sqrt{L_C/C_C}$ (Ω)

At $\omega_0 t = \pi$, the current i_{T_2} cannot reverse as the diode in series with T_2 is reverse bias and the voltage V_{C_C} across the commutation capacitor retains a charge of $-V_{DC}$.

2.2 Activation of the fault by switching T_4

Fig. 2*b* illustrates how the fault current rises. When T_4 is switched on at t_0 (with the others switches off), the energy stored in the capacitor bank C_{bank} is released through the load inductor L_C and fault resistor R_{FAULT} to produce a high current through the VCB before the electrodes separate. The commutation circuit is a second-order *L*–*C*–*R* circuit with a capacitor initial voltage of V_{DC}. The load resistor R_{LOAD} is ignored due to its large resistance compared with the fault resistor R_{FAULT}. The circuit loop comprising C_{bank}–VCB–L_{LOAD}–T_4–R_{FAULT} is expressed by

$$\frac{1}{C_{bank}}\int^{i_{FAULT}} \mathrm{d}t + L_{LOAD}\frac{\mathrm{d}i_{FAULT}}{\mathrm{d}t} + i_{FAULT}R_{FAULT} = 0 \tag{10}$$

with the initial conditions

$$i_{FAULT} = i_{VCB'} \simeq 0 \text{ (A)}; \quad V_{C_{bank}} = -V_{DC} \text{ (V)}$$

Equation (10) can be divided into three different models in term of the relationship between R_{FAULT} and $2\sqrt{L_{LOAD}/C_{bank}}$.

When $R_{FAULT} > 2\sqrt{L_{LOAD}/C_{bank}}$, it is an over-damped circuit, such that there are two unequally negative real numbers in its latent root. Thus, it yields

$$i_{FAULT}(t) = -\frac{V_{DC}}{L_{LOAD}(P_2 - P_1)}\left(\mathrm{e}^{p_1 t} - \mathrm{e}^{p_2 t}\right) \quad \text{(A)} \tag{11}$$

and

$$V_{C_{bank}}(t) = \frac{V_{DC}}{(P_2 - P_1)}\left(P_2\,\mathrm{e}^{p_1 t} - P_1\,\mathrm{e}^{p_2 t}\right) \quad \text{(V)} \tag{12}$$

where

$$P_1 = -\frac{R_{FAULT}}{2L_{LOAD}} + \sqrt{\left(\frac{R_{FAULT}}{2L_{LOAD}}\right)^2 - \frac{1}{L_{LOAD}C_{bank}}}$$

$$P_2 = -\frac{R_{FAULT}}{2L_{LOAD}} - \sqrt{\left(\frac{R_{FAULT}}{2L_{LOAD}}\right)^2 - \frac{1}{L_{LOAD}C_{bank}}}$$

The capacitor bank C_{bank} always discharges its stored energy into the fault path. When $t = 0_+$, $i_{FAULT}(0_+) = 0$; as $t \to \infty$, $i_{FAULT}(\infty) = 0$. Thus, the fault current must rise from zero and then decrease to zero; and time t_m to reach the maximum current, is determined from $\mathrm{d}i_{FAULT}/\mathrm{d}t = 0$, and is given by

$$t_m = \frac{\ln(P_2/P_1)}{P_1 - P_2} \tag{13}$$

Since the opening speed of the VCB is found to be about 1 m/s and the occurrence of the arc voltage indicates the contacts of the VCB starts to separate [9, 10], the time difference between t_1 and t_2 determines how far the internal electrodes have separated. Independent of the discharge mode, the commutation circuit current (having triggered T_3) has to rise to (or exceed) the fault current $i_{FAULT}(t)$ level at t_2, in order to be able to investigate VCB interruption properties. When the electrodes start to open at t_1, the VCB experiences an arc voltage, the polarity of which depends on the direction of the VCB current, until a successful commutation is achieved.

2.3 Commutation of the VCB by switching T_3

In Fig. 2*c*, the commutation period $t_2 - t_3$ is far shorter than the fault path time constant, and it is assumed that the fault current $i_{FAULT}(t)$is constant within this period. T_3 is fired to introduce the counter-current flow through the VCB, forcing the fault current through the VCB to zero, once the electrodes have separated to a specific distance. During this interval, the relationship between i_{FAULT}, i_{VCB} and i_{T_3} is given by

$$i_{FAULT} = i_{VCB} + i_{T_3} \quad \text{(A)} \tag{14}$$

where the differential equation for i_{T_3} is the same but with opposite direction to i_{T_2} during commutation and is given by

$$\frac{1}{C_C}\int^{i_{T_3}} \mathrm{d}t + L_C\frac{\mathrm{d}i_{T_3}}{\mathrm{d}t} = 0 \tag{15}$$

with the initial conditions

$$i_{T_3} = 0 \text{ (A)} \quad \text{and} \quad V_{C_C} = V_{DC} \text{ (V)}$$

which yields

$$i_{T_3}(t) = \frac{V_{DC}}{Z}\sin\omega_0 t \quad \text{(A)} \tag{16}$$

and

$$\begin{gathered} V_{C_C}(t) = V_{DC}\cos\omega_0 t \quad \text{(V)} \\ 0 \le \omega_0 t \le \pi \quad \text{(rad)} \end{gathered} \tag{17}$$

where $\omega_0 = 1/\sqrt{L_C C_C}$ (rad/s) and $Z = \sqrt{L_C/C_C}$ (Ω)

With the appropriate choice of L_C and C_C, that is, with an appropriate selection of d*i*/d*t*, a successful interruption should occur as a result of the first CZ. The second CZ is utilised if the first interruption fails. As the auxiliary switches (T_3 and T_4) are uni-directional due to the series blocking diodes thereby preventing the current reversing, the counter-current introduced by the resonant $L_C C_C$ circuit can produce at most two CZs as its amplitude exceeds the VCB current at the time of commutation, thus providing two opportunities for an interruption. The interruption process is considered a failure if the VCB current continues after the second gap CZ (this is similar to AC breakers which can be specified based on two mains cycles for commutation). It is assumed that interruption is achieved at first CZ, which means $i_{T_3}(t_3) = i_{FAULT}(t_2, t_3)$. The time t_{CZ1} to the first VCB CZ is

$$t_{CZ1} = \frac{-\sin^{-1}\{i_{FAULT}(t_2)Z/V_{DC}\}}{\omega_0} \tag{18}$$

The timesingledollar singledollar to the second VCB CZ is

$$t_{CZ2} = \frac{\pi + \sin^{-1}\{i_{FAULT}(t_2)Z/V_{DC}\}}{\omega_0}$$

The VCB voltage falls to and is clamped to the residual voltage of the commutation capacitor. Thus, the fault current passing through the VCB is commutated into the $L_C - C_C$ path; and the current $i_{T'_3}$ in the circuit loop C_{bank}–C_C–T_3–L_C–L_{LOAD}–T_4–R_{FAULT} is defined by

$$\frac{1}{C_C}\int^{i_{T'_3}} \mathrm{d}t + L_C\frac{\mathrm{d}i_{T'_3}}{\mathrm{d}t} + L_{LOAD}\frac{\mathrm{d}i_{T'_3}}{\mathrm{d}t} + i_{T'_3}R_{FAULT} = V_{DC} \quad (19)$$

where the voltage across C_{bank} can be considered a DC source due to a large C_{bank} with the initial conditions

$$i_{T'_3} = i_{T_3}(t_3)\ (A) \quad \text{and} \quad V_{C'_C} = V_{C_C}(t_3)\ (V)$$

Practically, $R_{FAULT} < 2\sqrt{L_{LOAD}/C_C}$. Thus, (19) yields

$$i_{T'_3}(t) = 2K_1\,\mathrm{e}^{-\delta_2 t}\cos(\omega_3 t - \theta) \quad (A) \quad (20)$$

$$V_{C'_C}(t) = \frac{2K_1}{C_C\omega_4}[\cos(\beta_2 - \theta) - \mathrm{e}^{-\delta_2 t}\cos(\omega_3 t - \theta + \beta_2)] + V_{C_C}(t_3)\ (V) \quad (21)$$

where

$$\delta_2 = \frac{R_{FAULT}}{2(L_{LOAD}+L_C)};$$

$$\omega_3^2 = \frac{1}{(L_{LOAD}+L_C)C_C} - \left(\frac{R_{FAULT}}{2(L_{LOAD}+L_C)}\right)^2;$$

$$\omega_4 = \sqrt{{\delta_2}^2 + \omega_3^2}; \quad \beta_2 = \tan^{-1}\frac{\omega_3}{\delta_2};$$

$$K_1 = \sqrt{\left(\frac{i_{T_3}(t_3)}{2}\right)^2 + \left(\frac{[\{V_{DC} - V_{C_C}(t_3)\}/\{L_{LOAD}+L_C\}] - \delta_2 i_{T_3}(t_3)}{2\omega_3}\right)^2};$$

and

$$\theta = \tan^{-1}\frac{[\{V_{DC} - V_{C_C}(t_3)\}/\{L_{LOAD}+L_C\}] - \delta_2 i_{T_3}(t_3)}{\omega_3 i_{T_3}(t_3)}$$

During interval t_3–t_5, the current $i_{T'_3}$ initially increases due to the stored magnetic energy transfer and the residual voltage on the commutation capacitor. Then it starts to reduce, allowing diode D_{FW} to conduct; whence the voltage across the VCB reaches its maximum voltage V_{DC} thereby forward biasing the freewheel diode.

With diode D_{FW} forward bias, the load (the fault) is bypassed, effectively decoupling the fault from the commutation circuit. Current $i_{T'_3} = i_{T''_3} + i_{FW}$, where $i_{T''_3}$ discharges through the circuit loop C_{bank}–C_C–T_3–L_C–D_{FW}, transferring magnetic energy to an electric field, causing V_{C_C} to increase according to

$$\frac{1}{C_C}\int^{i_{T''_3}} \mathrm{d}t + L_C\frac{\mathrm{d}i_{T''_3}}{\mathrm{d}t} = V_{DC} \quad (22)$$

with the initial conditions

$$i_{T''_3} = i_{T'_3}(t_5)\ (A) \quad \text{and} \quad V_{C''_C} = V_{C'_C}(t_5)\ (V)$$

which yields

$$i_{T''_3}(t) = \frac{V_{DC} - V_{C'_C}(t_5)}{Z}\sin(\omega_0 t) + i_{T'_3}(t_5)\cos(\omega_0 t) \quad (A) \quad (23)$$

$$V_{C''_C}(t) = \left[V_{DC}\cos(\omega_0 t) - V_{C'_C}(t_5)(\cos(\omega_0 t) - 1) + Z i_{T'_3}(t_5)\sin(\omega_0 t)\right] \quad (24)$$

where $\omega_0 = 1/\sqrt{L_C C_C}$ (rad/s) and $Z = \sqrt{L_C/C_C}$ (Ω)

The voltage V_{C_C} across the commutation capacitor terminates with the opposite polarity, when current $i_{T''_3}$ reduces to zero. The transfer of the stored magnetic energy in L_C causes this voltage rise. The time t_d, t_5 to t_6, is

$$t_d = \frac{1}{\omega_0}\tan^{-1}\frac{i_{T'_3}(t_5)Z}{V_{DC} - V_{C_C'}(t_5)} \quad (25)$$

As the current $i_{T''_3}$ reduces to zero at t_6, the current i_{FW} conducts through the circuit loop L_{LOAD}–T_4–R_{FAULT}–D_{FW} to dissipate the magnetic energy stored in the load (fault) inductor L_{LOAD}, which obeys the following differential equation

$$L_{LOAD}\frac{\mathrm{d}i_{FW}}{\mathrm{d}t} + R_{FAULT}i_{FW} = 0 \quad (A) \quad (26)$$

with the initial conditions

$$i_{FW}(t_6) = i_{T_3'}(t_6)$$

which yields

$$i_{FW}(t) = i_{T_3'}(t_6)\,\mathrm{e}^{(-t/\tau_3)}$$

where $\tau_3 = L_{LOAD}/R_{FAULT}$

The analytical equations corresponding to each interval of the test circuit have now been derived. They can be used to calculate the required peak voltage, peak currents and the CZ time when the component values and conditions are known; such as when the commutation circuit is triggered to achieve a CZ.

3 Simulation results

A typical interruption failure occurs when the counter-current produced by the commutation circuit is less than the fault current due to slow detection and triggering of the solid-state switches. That is, there is no CZ in the VCB. The commutation parameters are initially deliberately designed to result in an unsuccessful interruption. Fig. 3*a* gives the simulated results overview. Fig. 3*b* depicts the simulation in more detail, and the preparation and interruption of the test circuit. The figures on the left describe the voltage across capacitor bank $V_{C_{bank}}$, the commutation capacitor V_{C_C} and the main switch V_{VCB}. The figures on the right plot the current passing through the main switch i_{VCB}, the fault path i_{FAULT}, the resistor R_1 path i_1, the commutation T_2 path i_{T_2} and T_3 path i_{T_3}. A failed interruption induced by large di/dt and dv_{VCB}/dt can be simulated, as shown in Figs. 3*c* and *d*. With high di/dt and dv_{VCB}/dt, the current passing through the VCB still conducts even if CZ points occur. The model of the VCB is seen as a short circuit in this situation [19, 20].

Test circuit performance during a successful interruption at the first CZ is shown in Fig. 4. Fig. 4*a* shows the overall view and Fig. 4*b* depicts the results in detail. The waveforms on the left are voltage profile, while current profile is on the right.

During successful interruption, the energy stored in the inductance is transferred so as to contribute to the V_{C_C} increase. In Fig. 4, V_{VCB} immediately equals V_{C_C} when the first CZ occurs and then tracks its change until the free-wheel diode D_{FW} conducts.

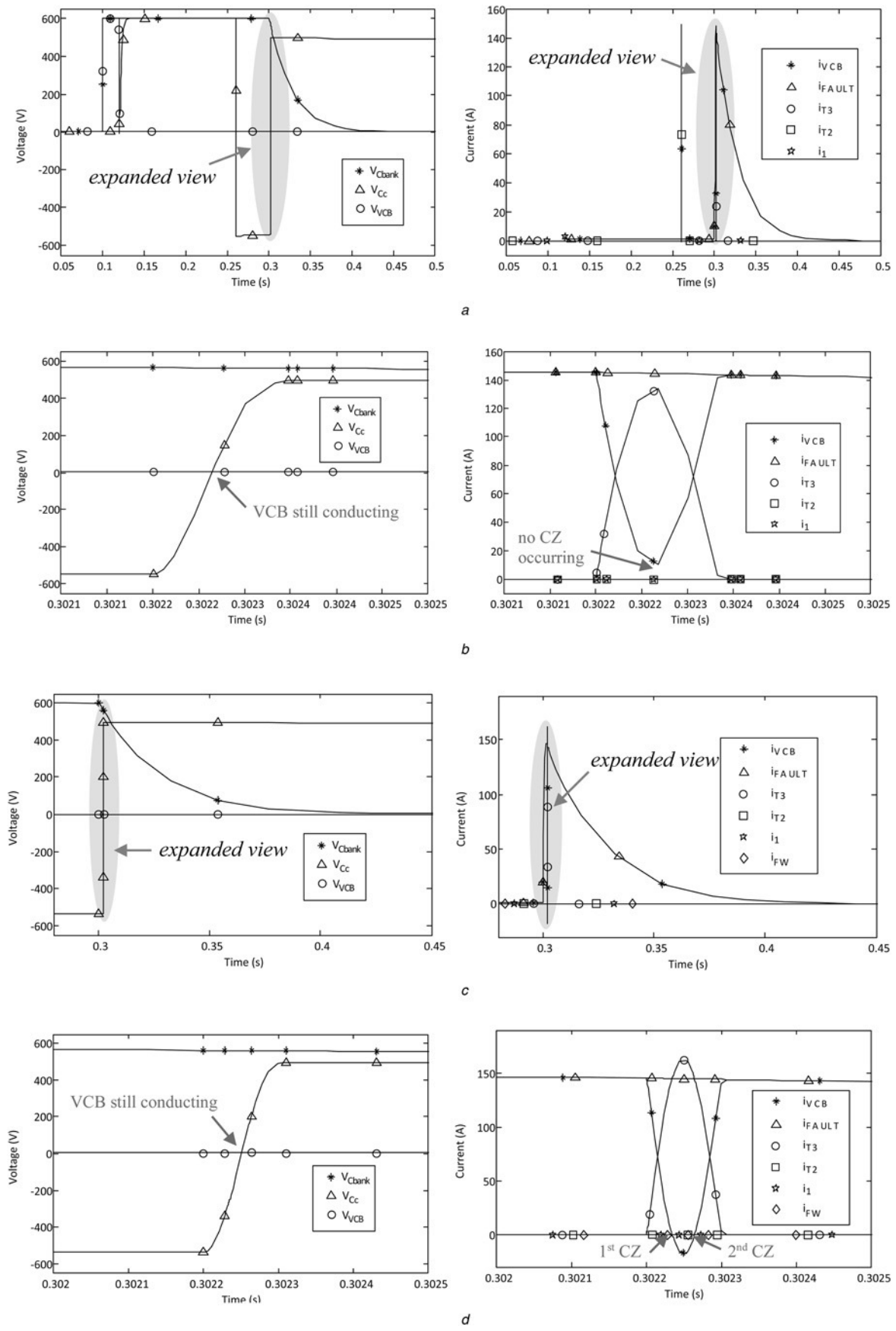

Fig. 3 *Test circuit simulation waveforms for unsuccessful interruption*

a Overview of simulated results on no CZ condition
b Detailed view on respective waveforms with no CZ condition
c Overview of simulated results on large di/dt and dV_{VCB}/dt condition
d Detailed view on respective waveforms with large di/dt and dV_{VCB}/dt condition
$V_{DC} = 600$ V, $C_{bank} = 7$ mF, $C_C = 10$ µF, $R_1 = 200$ Ω, $L_C = 150$ µH, $L_{LOAD} = 1.7$ mH, $R_{LOAD} = 600$ Ω, $R_{FAULT} = 4$ Ω

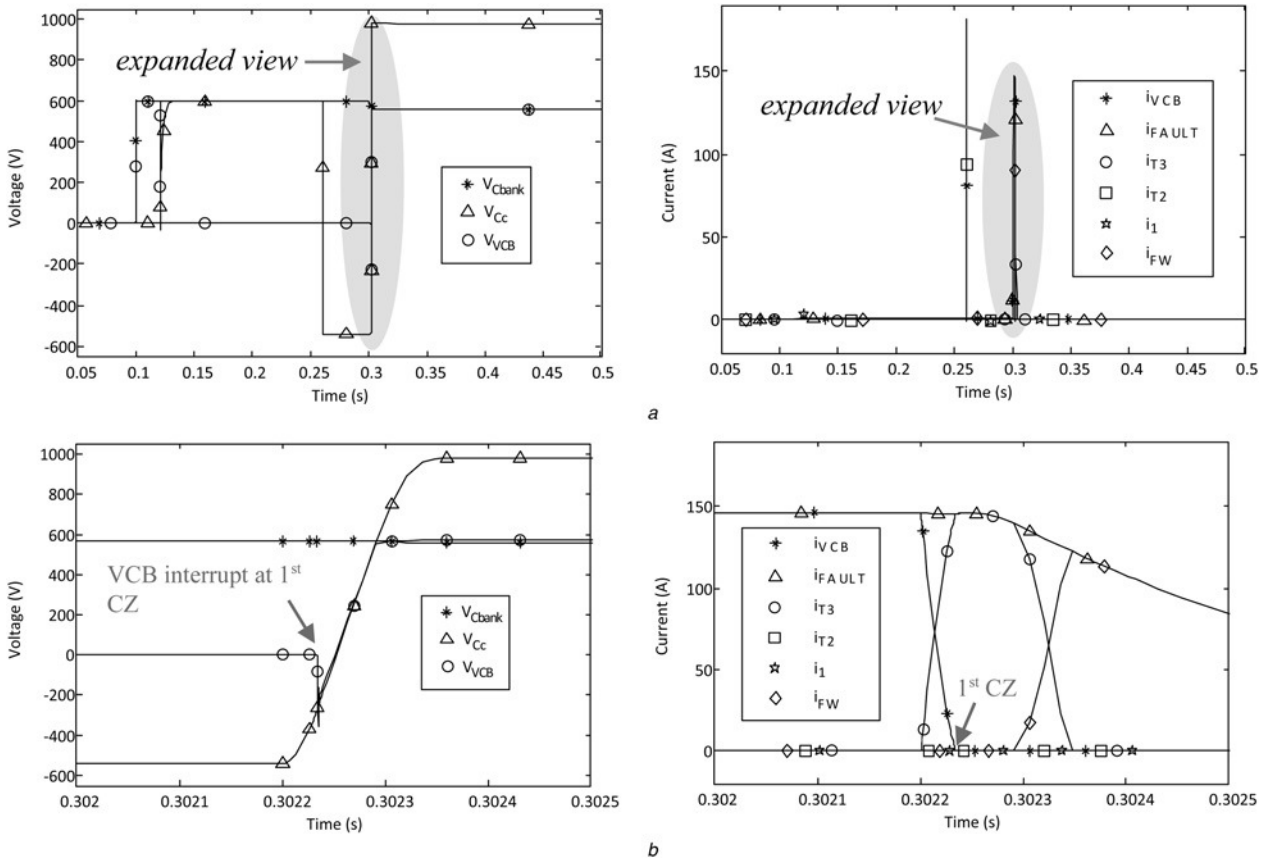

Fig. 4 *Test circuit simulation waveforms for successful interruption*

a Overview of simulated results with first CZ condition
b Detailed view on respective waveforms with first CZ condition
$V_{DC} = 600$ V, $C_{bank} = 7$ mF, $C_C = 10$ µF, $R_1 = 200$ Ω, $L_C = 150$ µH, $L_{LOAD} = 1.7$ mH, $R_{LOAD} = 600$ Ω, $R_{FAULT} = 4$ Ω

4 Experimental results

Test circuit experimentation is necessary to validate the analysis and simulation results, and also to explore VCB interruption in terms of external conditions, including di/dt and dv_{VCB}/dt. Interruption probability is based on the successful interruption at either of first two CZ points. To avoid system damage due to the effects of excessive currents, an MOV was connected across the VCB and a series diode was located before capacitor bank ($C_{bank} = 7$ mF) to block currents flowing back into the DC source. 600 Ω load resistance was utilised in all the experimentation. The VCB characteristics are shown in Table 2.

The performance of the test circuit interrupting a 330 A fault current at the first CZ is shown in Fig. 5*a*. After the voltage V_{C_C} across commutation capacitor reversed and retained as described in Section 2.1, the fault current i_{FAULT} produced by the capacitor bank voltage $V_{C_{bank}}$ is actuated and flows through the VCB before electrode separation, so $i_{FAULT} = i_{VCB}$. The fault current through the VCB is sinusoidally displaced by the commutation circuit current i_{T_3}, until the VCB current is zero; when $i_{FAULT} = i_{T_3}$ and $i_{VCB} = 0$. During this period, the voltage across the VCB (V_{VCB}) is zero initially due to the electrodes being closed and when parting, a constant 12 V arc forms as i_{FAULT} rises. As long as the di/dt (rate of change of the VCB current before CZ) was appropriately designed or the gap distance of the VCB reaches to a specific value to support a large di/dt, the commutation will be successful and the gap voltage clamps to the capacitor residual voltage V_{C_C}, until i_{T_3} starts to decrease (D_{FW} conduction). V_{VCB} has been charged to V_{DC} but V_{C_C} continues to increase due to the energy stored in the commutation inductor L_C.

The corresponding parts of Fig. 5*b* show interruption at the second gap CZ with the same interrupting current level. In this case, i_{VCB} continues to flow through the VCB in the opposite direction. The arc voltage V_{VCB} 12 V is reverse. Finally, the interruption is successful at the second CZ. With successive interruption attempts the resonance voltage in V_{VCB} progressively decays, since resistance is introduced as the plasma starts to recover. Oscillation with the commutation inductor occurs after a successful interruption because of a VCB gap capacitive effect [21].

The voltage performance during an unsuccessful interruption is shown in Fig. 6*a*, with the corresponding current waveforms in the expanded view. Interruption failure occurrence is random; sometimes, even with successful interruption conditions at the first or second CZ, failure occurs without any electrical visual indication, as shown in Figs. 6*a* and *b*. The reason for re-ignition is that there is no vacuum state in the vacuum interrupter after CZ or parts of the contacts are still able to emit vapour because of a hot spot on electrode surface after experiencing the arc. In other words, the arc starts to recover as its current is reduced, but recovery speed is determined by a recovery rate. For a given gap, if di/dt is slightly more than the recovery rate, interruption is possible. However, if di/dt significantly exceeds the recovery rate,

Table 2 Technical data on triple pole VCBs [21]

Contactor reference	CMV 15
operating voltage, kV	1.2
current rating, A	150
max motor duty, kW	225
max transformer duty, kVA	250
closing, W	250
hold in, W	12
weight of contactor, kg	4
thermal rating (1 s), kA	4
mechanical life, cycles	5×10^6

IET Power Electron., 2016, Vol. 9, Iss. 2, pp. 207–218

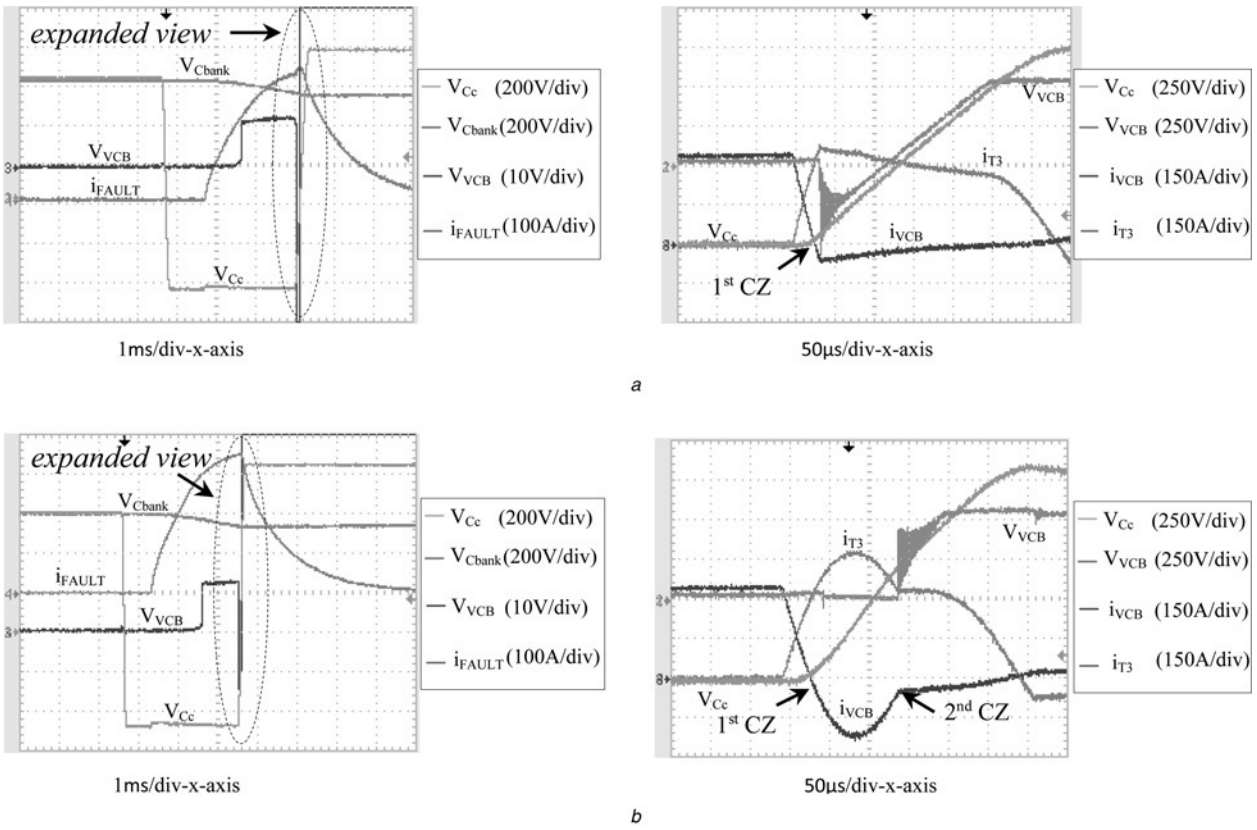

Fig. 5 *Test circuit experimental waveforms for successful interruption*

a Experimental waveforms for successful interruption at the first CZ; $L_C = 49.4$ µH, $C_C = 76.67$ µF
b Experimental waveforms for successful interruption at the second CZ; $L_C = 36.87$ µH, $C_C = 32.05$ µF
$I_{FAULT} = 330$ A, $V_{DC} = 600$ V, $L_{LOAD} = 1.7$ mH, $R_{FAULT} = 1.7$ Ω

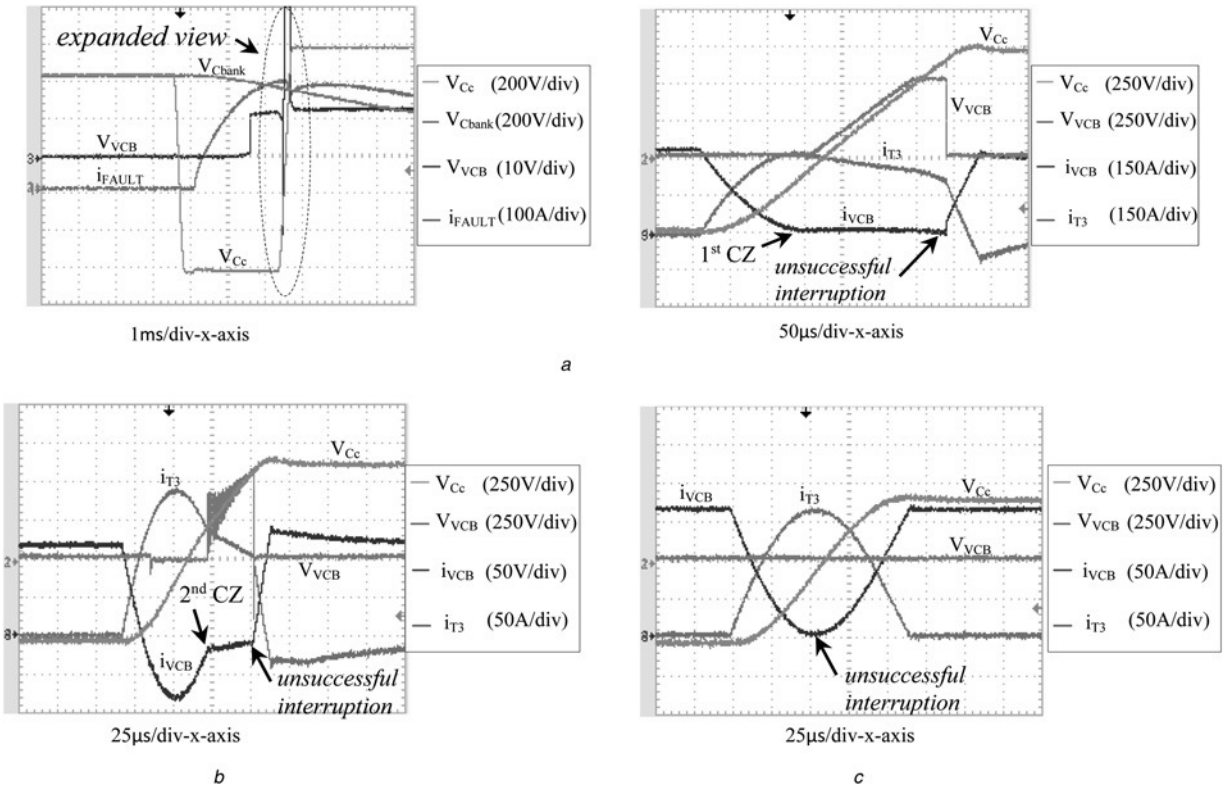

Fig. 6 *Experimental waveforms for unsuccessful interruption at first and second CZ, with too large fault current*

a Experimental waveforms for unsuccessful interruption after the first CZ; $I_{FAULT} = 330$ A, $L_C = 131.96$ µH, $C_C = 76.67$ µF
b Experimental waveforms for unsuccessful interruption after the second CZ; $I_{FAULT} = 170$ A, $L_C = 99$ µH, $C_C = 12.8$ µF
c Experimental waveforms for unsuccessful interruption without first CZ; $I_{FAULT} = 170$ A, $L_C = 99$ µH, $C_C = 12.8$ µF
$V_{DC} = 600$ V, $L_{LOAD} = 1.7$ mH, $R_{FAULT} = 1.7$ Ω

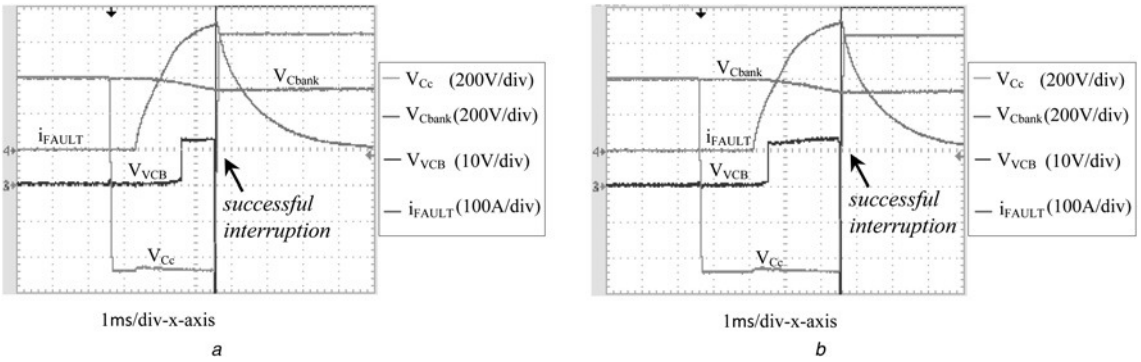

Fig. 7 *Experimental waveforms for successful interruptions with same interrupting current but different gap distance*

a Gap distance 1 mm
b Gap distance 2 mm
$I_{FAULT} = 330$ A, $V_{DC} = 600$ V, $L_C = 36.87$ μH, $C_C = 32.05$ μF, $L_{LOAD} = 1.7$ mH, $R_{FAULT} = 1.7$ Ω

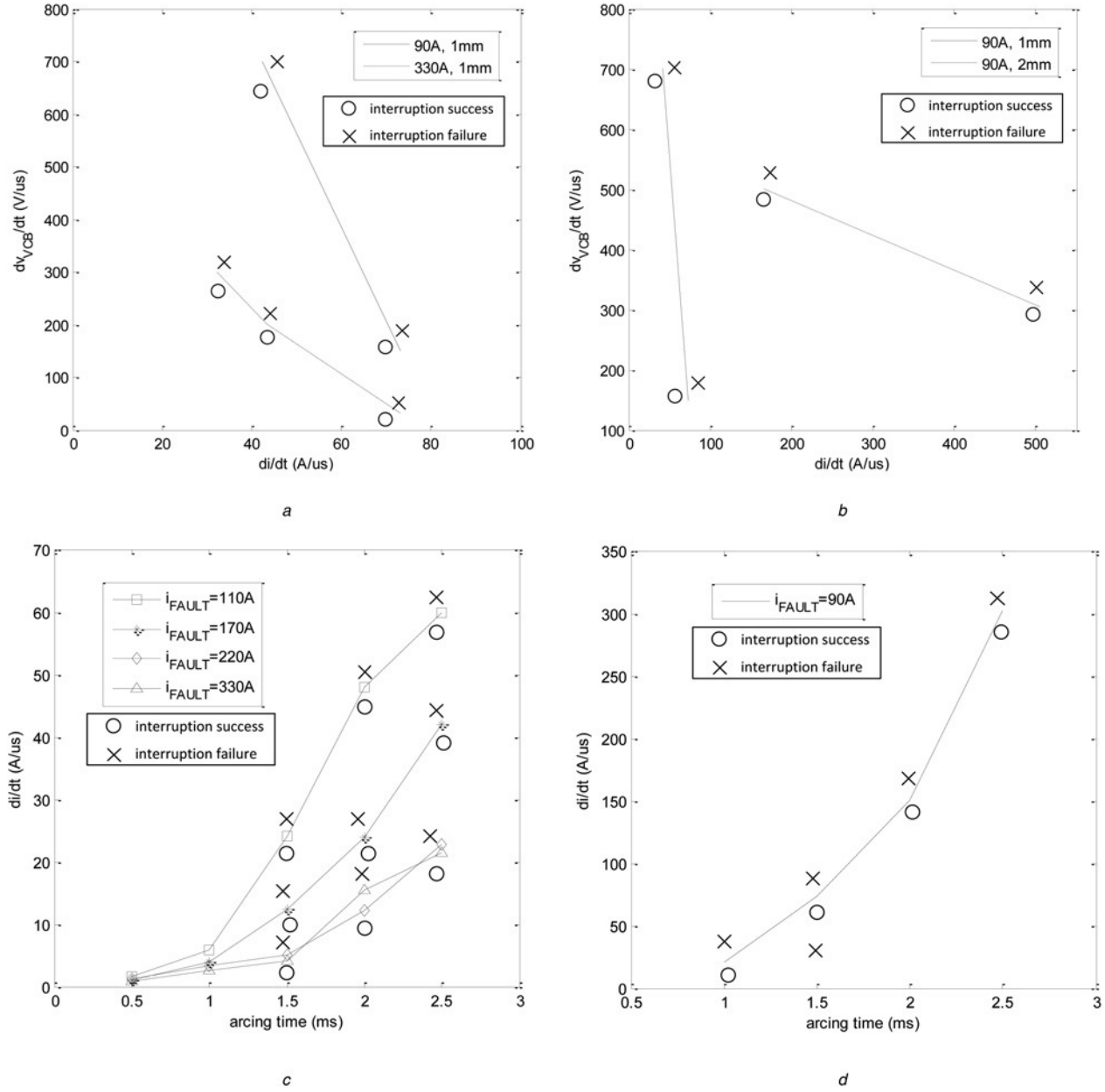

Fig. 8 *VCB interruption characteristics*

a Relationship between d*i*/d*t* and dV_{VCB}/d*t* with 1 mm gap distance; $I_{FAULT} = 90$ and 330 A
b Relationship between d*i*/d*t* and dV_{VCB}/d*t* with 1 and 2 mm gap distance; $I_{FAULT} = 90$ A
c Relationship between varied interruption current, d*i*/d*t* and arcing time with 1 mm gap distance; $I_{FAULT} = 110$, 170, 220 and 330 A
d Relationship between varied interruption current, d*i*/d*t* and arcing time with 1 mm gap distance; $I_{FAULT} = 90$ A

IET Power Electron., 2016, Vol. 9, Iss. 2, pp. 207–218

interruption becomes impossible. Failed interruption due to a peak i_{T_3} that does not realise a CZ in i_{VCB} is shown in Fig. 6*c*.

After electrode separation, the VCB maintains stable movement with an opening speed of about 1 m/s. The occurrence of the arc voltage could be considered as the separation point of the VCB internal electrodes if the interruption current is low for a given VCB. This means the period of the arc voltage is related to the how far the electrodes have parted. With adjustment of the control signals as shown in Fig. 1, the delay is controlled by varying time between t_1 and t_2. That is, this determines the vacuum gap at point that commutation starts. Thus, the VCB can be interrupt at the same current level for different gap distances, by adjustment of the control signals as shown in Fig. 7. In this figure, the time between V_{C_c} been reversed and the occurrence of arc voltage is fixed at 2 ms, but the time to trigger i_{FAULT} is variable; hence interruption at gap distances 1 and 2 mm are shown in Fig. 7*a* and Fig. 7*b*, respectively.

The VCB characteristics in terms of the relationship between di/dt and dv_{VCB}/dt were investigated with interruption currents of 90 and 330 A at arcing times of 1 and 2 ms. Based on the fixed delay time as shown in Fig. 7, Fig. 8*a* illustrates the results with interruption currents of 90 and 330 A at a gap distance of 1 mm. The results for interruption at gap distances 1 and 2 mm with interruption current 90 A are shown in Fig. 8*b*. Interruption success and failure are represented by the symbol circles and crosses, respectively. The lines indicate the boundary between successful and failed interruption (the area above each lines is the failed interruption zone). The experimental conditions are shown in Table 3. The experiments were repeated at least 30 times for every value. i_{FAULT} is the interruption current; $g$is gap length; di/dt is rate of change of the VCB current before CZ; dv_{VCB}/dt is the VCB voltage immediately after CZ.

With the same di/dt, the dv_{VCB}/dt in interrupting 330 A is small than when interrupting 90 A. At 1 mm, although some dv_{VCB}/dt are large compared with those at 2 mm, the di/dt generally presents a small value. Regardless of interrupting 90 and 330 A or with a gap distance of 1 and 2 mm, in obtaining 100% interruption probability, an increase in di/dt requires a decrease in dv_{VCB}/dt. However, di/dt cannot increase even if it is aided by a decrease in dv_{VCB}/dt.

An experiment interrupting 330 A at a 1 mm gap was carried out. The result indicated that the interruption probability can reach 100% when di/dt is reduced to 2.53 A/μs. The VCB interruption characteristics were investigated with varying interruption current, di/dt, and arcing time, with results shown in Figs. 8*c* and *d*. The interruption success and failure are indicated by the symbol circles and crosses, respectively. The boundaries between successful and failed interruption are denoted by solid lines (above the line is the failed interruption zone). The experimental conditions are tabulated in Table 4 and the experiments were repeated at least 30 times for the test.

As shown in Fig. 8*c*, with a small arcing time, the di/dt's asymptote regardless of the interruption current level. For a large arcing time, the interruption limit current increases with decreasing di/dt. The reason seems that the dielectric strength increases as the gap volume is increased [22]. Fig. 8*d* shows that a failed interruption could occur with a low probability (about 1 in 30 times) even if the di/d$t$is low. The successful interruption of the VCB is very sensitive to di/dt, dv_{VCB}/dt and interruption current level. In addition, all these factors vary among VCBs. With *LC* commutation circuit, the peak value of the counter-current produced is larger than the fault current, therefore introducing at most two

Table 3 Experimental conditions for di/dt–dv_{VCB}/dt characteristic

i_{FAULT}, A	g, mm	di/dt, A/μs	dv_{VCB}/dt, V/μs
90	1	73.18	187.5
		40.68	692.3
	2	398.6	300
		201.4	500
330	1	70	47.14
		41.92	194.1
		36.39	300

Table 4 Experimental conditions for interruption characteristics

i_{FAULT}, A	di/dt, A/μs				
	g, mm				
	0.5	1	1.5	2	2.5
90	–	20.5	73.27	150.5	302.5
110	1.69	5.86	21.97	47.62	61.34
170	1.29	3.85	12.5	24.93	42.03
220	1.19	3.29	5.05	12.3	22.78
330	0.89	2.53	4.08	15.55	21.41

CZs with different interruption current level. The interruption current is equal to the fault current during the first CZ. The interruption current level is smaller at second CZ. When the di/dt at first CZ is too large resulting in failure interruption, successful interruption will occurs at second CZ as current level has reduced.

5 Conclusion

An active commutation test circuit is proposed in this paper to investigate VCB properties in terms of varied interruption current, di/dt, dv_{VCB}/dt and arcing time. The experimental results confirmed that VCB interruption performance at low power rating is similar to that at high power rating. A decrease in di/dt or dv_{VCB}/dt increases the interruption probability. Based on a fixed di/dt, dv_{VCB}/dt and arcing time, the interruption probability is inversely proportional to the interruption current. di/dt and dv_{VCB}/dt for successful interruption reduce with decreased electrode spacing. However, the key parameter determining interruption probability is di/dt, where even if dv_{VCB}/dt is low, successful interruption become impossible if the di/dt is above certain level. In addition, the performance of the proposed active commutation test circuit offers the following features:

- There is no need for a continuous external voltage to charge the commutation capacitor C_C: it is charged from the system voltage.
- There is no need for large capacitance C_C, since the interruption time is reduced.
- With an optimally designed commutation circuit, the interruption probability is improved and the extra time for commutation can be compensated by early triggering. Electrode surface erosion is reduced, thus the useful life of the VCB is extended.

An accurate VCB model is not presented in this paper, whereas the VCB model used in this paper attempt to retain the features and regular pattern of successful VCB interruptions based on external conditions. Although this approach is useful in the fault current interruption analysis, an accurate VCB model will be useful in system level analysis and the simulation of the vacuum arc interruption. Further investigation on the VCB model is recommended. Current investigation to improve the VCB interruption during t_2–t_6 intervals are ongoing with the proposed test circuit topology.

6 Acknowledgments

The authors gratefully acknowledge the support of EPSRC grant EP/K035096/1: Underpinning Power Electronics 2012 - Converters theme.

7 References

1 Andersson, D., Henriksson, A.: 'Passive and active DC breakers in the three Gorges–Changzhou HVDC project'. Proc. of Int. Conf. on Power Systems, 2001, pp. 391–395

2 Arimatsu, K., Yoshioka, Y., Tokuyama, S., *et al.*: 'Development and interrupting tests on 250 KV 8 KA HVDC circuit breaker', *IEEE Trans. Power Appar. Syst.*, 1985, **PAS-104**, pp. 2452–2459

3 Pauli, B., Ruoss, E., Mauthe, G., *et al.*: 'Development of a high current HVDC circuit breaker with fast fault clearing capability', *IEEE Trans. Power Deliv.*, 1988, **3**, pp. 2072–2080
4 Pucher, W.: 'Fundamentals of HVDC interruption', *Electra*, 1968, ELT_005_1 pp. 24–38
5 Premerlani, W.J.: 'Forced commutation performance of vacuum switches for HVDC breaker application', *IEEE Trans.*, 1982, **PAS-101**, pp. 2721–2727
6 Kontos, E., Teixeira, R., Rodrigues, S., *et al.*: 'Impact of HVDC transmission system topology on multi-terminal DC network faults', *IEEE Trans. Power Deliv.*, 2015, **30**, (2), pp. 844–852
7 Sneath, J., Rajapakse, A.: 'Fault detection and interruption in an earthed HVDC grid using ROCOV and hybrid DC breakers', *IEEE Trans. Power Deliv.*, doi: 10.1109/TPWRD.2014.2364547, IEEE Early Access Articles, 2014, 99, p. 1
8 Derakhshanfar, R., Jonsson, T., Steiger, U., *et al.*: 'Hybrid HVDC breaker-a solution for future HVDC system' (CIGRE, 2014)
9 Hassanpoor, A., Hafner, J., Jacobson, B.: 'Technical assessment of load commutation switch in hybrid HVDC breaker', *IEEE Trans. Power Electron.*, doi:10.1109/TPEL.2014.2372815, 2015, **30**, pp. 5393–5400
10 ABB: 'The hybrid HVDC breaker an innovation breakthrough enabling reliable HVDC grids'. Available at http://www05.abb.com/global/scot/scot221.nsf/veritydisplay/c9d5ba256e7e9671c1257ab6004b1feb/$file/hybrid-hvdc-breaker-an-innovation-breakthrough-for-reliable-hvdc-gridsnov2012.pdf
11 ABB: 'Patent US 2013/0070492', High Voltage DC Breaker Apparatus, 21 March 2013
12 Eriksson, T., Backman, M., Halen, S.: 'A low loss mechanical HVDC breaker for HVDC grid applications' (CIGRE, Paris, 2014)
13 Tahata, K., Ka, S., Tokoyoda, S., *et al.*: 'HVDC circuit breakers for HVDC grid applications'. AORC Technical Meeting, 2014, pp. 1–8
14 Tahata, K., El Outkaili, S., Kamei, K., *et al.*: 'HVDC circuit breakers for HVDC grid applications'. IET ACDC 2015 Conf., 2015
15 Franck, C.M.: 'HVDC circuit breakers: a review identifying future research needs', *IEEE Trans. Power Deliv.*, 2011, **26**, pp. 998–1007
16 Odaka, H., Yamada, M., Sakuma, R., *et al.*: 'DC interruption characteristic of vacuum circuit breaker', *Electr. Eng. Jpn*, 2007, **161**, pp. 17–25
17 Niwa, Y., Matsuzaki, J., Yokokura, K.: 'The basic investigation of the high-speed VCB and its application for the DC power system'. 23rd Int. Symp. on Discharges and Electrical Insulation in Vacuum, 2008, ISDEIV 2008, 2008, vol. 1, pp. 107–112
18 Niwa, Y., Funahashi, T., Yokokura, K., *et al.*: 'Basic investigation of a high-speed vacuum circuit breaker and its vacuum arc characteristics', *IEE Proc., Gener. Transm. Distrib.*, 2006, **153**, pp. 11–15
19 Greenwood, A.N., Lee, T.H.: 'Theory and application of the commutation principle for HVDC circuit breakers', *IEEE Trans. Power Appar. Syst.* 1972, **PAS-91**, pp. 1570–1574
20 Greenwood, A.N., Barkan, P., Kracht, W.C.: 'HVDC vacuum circuit breakers', *IEEE Trans. Power Appar. Syst.*, 1972, **PAS-91**, pp. 1575–1588
21 Wallacetown, A.: 'Vacuum contactors', August 2008, pp. 1–6
22 van Lanen, E., Smeets, R., Popov, M., *et al.*: 'Vacuum circuit breaker postarc current modelling based on the theory of Langmuir probes', *IEEE Trans. Plasma Sci.*, 2007, **35**, pp. 925–932